Self-Similar Nanocavity Design with Ultrasmall Mode Volume for Single-Photon Nonlinearities

Self-Similar Nanocavity Design with Ultrasmall Mode Volume
for Single-Photon Nonlinearities

Hyeongrak Choi,[1,*] Mikkel Heuck,[1,2] and Dirk Englund[1,†]

[1]*Research Laboratory of Electronics, Massachusetts Institute of Technology, Cambridge, Massachusetts 02139, USA*
[2]*Department of Photonics Engineering, Technical University of Denmark, 2800 Kgs. Lyngby, Denmark*
(Received 30 December 2016; published 30 May 2017)

We propose a photonic crystal nanocavity design with self-similar electromagnetic boundary conditions, achieving ultrasmall mode volume (V_{eff}). The electric energy density of a cavity mode can be maximized in the air or dielectric region, depending on the choice of boundary conditions. We illustrate the design concept with a silicon-air one-dimensional photon crystal cavity that reaches an ultrasmall mode volume of $V_{\text{eff}} \sim 7.01 \times 10^{-5}\lambda^3$ at $\lambda \sim 1550$ nm. We show that the extreme light concentration in our design can enable ultrastrong Kerr nonlinearities, even at the single-photon level. These features open new directions in cavity quantum electrodynamics, spectroscopy, and quantum nonlinear optics.

Optical nanocavities with small mode volume (V_{eff}) and high quality factor (Q) can greatly increase light-matter interaction [1] and have a wide range of applications including nanocavity lasers [2–4], cavity quantum electrodynamics [5,6], single-molecule spectroscopy [7], and nonlinear optics [8–10]. Planar photonic crystal cavities can enable high Q factors, exceeding 10^6 [11], together with mode volumes that are typically on the order of a qubic wavelength. However, it was shown that by introducing an air slot into a photonic crystal (PhC) cavity, it is possible to achieve the electromagnetic (EM) mode with small V_{eff} on the order of $0.01\lambda^3$ [12], where λ is the free-space wavelength. This field concentration results from the boundary condition on the normal component of the electric displacement ($\vec{D}$). Here, we propose a method to further reduce V_{eff} by making use of the second EM boundary condition, the conservation of the parallel component of the electric field. Furthermore, these field concentration methods can be concatenated to reduce V_{eff} even further, limited only by practical considerations such as fabrication resolution. The extreme field concentration of our cavity design opens new possibilities in nonlinear optics. In particular, we show that Kerr nonlinearities, which are normally weak, would be substantially enhanced so that even a single photon may shift the cavity resonance by a full linewidth, under realistic assumptions of materials and fabrication tolerances.

The mode volume of a dielectric cavity [described by the spatially varying permittivity $\epsilon(\vec{r})$] is given by the ratio of the total electric energy to the maximum electric energy density [13],

$$V_{\text{eff}} = \frac{\int \epsilon(\vec{r})|E(\vec{r})|^2 dV}{\max(\epsilon(\vec{r})|E(\vec{r})|^2)}. \qquad (1)$$

In typical PhC cavity designs, the minimum cavity mode volume is given by a half-wavelength bounding box, or

$V_{\text{eff}} \sim (\lambda/2n)^3$ [14], agreeing with the diffraction limit. However, as is clear from Eq. (1), the mode volume is determined by the electric energy density at the position where it is maximized. Thus, it is not strictly restricted by the diffraction limit. A strong local inhomogeneity in $\epsilon(\vec{r})$ can greatly increase this electric energy density and correspondingly shrink the mode volume.

Figure 1(a) plots the fundamental mode of a silicon-air one-dimensional PhC cavity produced by three-dimensional FDTD simulations. This mode pattern (represented here as $|E|$ at the cavity center plane, $z = 0$) is modified only weakly for small perturbations of $\epsilon(\vec{r})$ in the cavity center, and therefore serves to approximate the numerator of Eq. (1). Robinson *et al.* [12] were able to increase the maximum electric field term in the denominator of Eq. (1) by introducing a thin air slot in the cavity center. This concentration results from the boundary condition on the normal component of the electric displacement (called here the type-1 BC), as illustrated in Fig. 1(b),

$$\epsilon_l E_{l\perp} = D_{l\perp} = D_{h\perp} = \epsilon_h E_{h\perp}, \qquad (2)$$

$$E_{l\perp} = \frac{\epsilon_h}{\epsilon_l} E_{h\perp}, \qquad (3)$$

where ϵ_l and ϵ_h are the permittivities of the low and high index materials, respectively, and the subscript $\perp$ represents the normal component of the field with respect to the dielectric boundary. The maximum electric energy density is thus increased by a factor of

$$\frac{W_{e1}}{W_{e0}} = \frac{\epsilon_l|E_l|^2}{\epsilon_h|E_h|^2} \approx \frac{\epsilon_h}{\epsilon_l}, \qquad (4)$$

assuming the cavity electric field is highly polarized orthogonal to the slot. Because the numerator in Eq. (1)
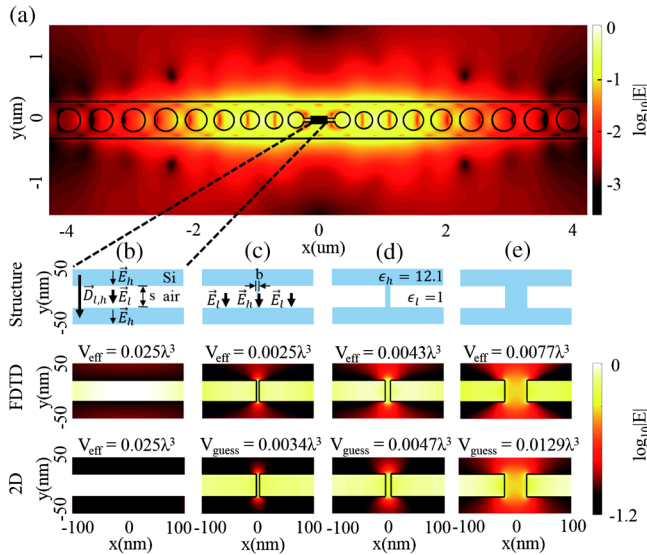
FIG. 1. Cavity field profiles of a slot cavity and slot-bridge (SB) cavities with different width of bridges. [(a) and (b)] Slot cavity achieving enhancement with the type-1 BC ($V_{eff} = 2.5 \times 10^{-2}\lambda^3$). Here, s denotes slot width, and $s = 40$ nm is used. [(c)–(e)] SB cavities achieving enhancement with type-2 BCs. Top: Index profile of the structure. Here, b denotes bridge width. Middle: Three-dimensional finite-difference time-domain (FDTD) simulation result. Bottom: Two-dimensional electrostatic simulation result. (c) $b = 5$ nm narrow bridge ($V_{eff} = 2.5 \times 10^{-3}\lambda^3$). (d) $b = 10$ nm intermediate bridge ($V_{eff} = 4.3 \times 10^{-3}\lambda^3$, $V_{guess} = 3.4 \times 10^{-3}\lambda^3$). (e) $b = 40$ nm wide bridge ($V_{eff} = 7.7 \times 10^{-3}\lambda^3$, $V_{guess} = 1.3 \times 10^{-2}\lambda^3$). For the V_{eff} calculation, electric energy density at the middle of the bridge is used as a maximum. This is because corners of the bridges produce a singularity of the field (suppressed by mesh size), but do not affect typical light-matter interaction. In other words, this is justified by overlap factors, for example, in the Purcell factor.

is roughly unchanged with the introduction of the thin air slot, V_{eff} is ultimately reduced by a factor of $\sim \epsilon_h/\epsilon_l$. Recently, Seidler *et al.* demonstrated a silicon-air PhC cavity with an air gap to reduce the cavity mode volume by a factor of 12.1 to $V_{eff} \sim 0.01\lambda^3$ [15]. The type-1 BC is wavelength independent, which provides some tolerance to fabrication imperfections. However, applications of this "air-mode cavity" design, which we define as a cavity with the highest electric energy density in the low-index medium, have been limited because the electric field is maximized in the low-index material.

Here, we introduce a method to further reduce V_{eff} by also making use of the boundary condition on the parallel component of the electric field (type-2 BC). A high-index bridge of width $b = 5$ nm is introduced across the slot of width $s = 40$ nm, as illustrated in Fig. 1(c). The parallel component of the electric field across this bridge is given by

$$E_{l\parallel} = E_{h\parallel}, \tag{5}$$

where $\parallel$ represents the parallel component of the electric field. Type-2 BC forces the electric field in the bridge to be same as that in the slot. Compared to the slot cavity, the maximum electric energy density is enhanced by a factor of

$$\frac{W_{e2}}{W_{e1}} = \frac{\epsilon_h|E_h|^2}{\epsilon_l|E_l|^2} \approx \frac{\epsilon_h}{\epsilon_l}. \tag{6}$$

For a vanishingly narrow bridge, the numerator of Eq. (1) is unchanged, so that V_{eff} is reduced by an additional factor of ϵ_h/ϵ_l. As opposed to the slot cavity, this modified design produces a "dielectric-mode cavity," defined as a cavity with the highest electric energy density in the high-index dielectric. This type of cavity enables enhanced light-matter interactions with embedded emitters or the bridge material itself that could not be covered by a slot cavity.

What happens if the bridge has finite width? For the $b = 5$ nm bridge shown in Fig. 1(c), our FDTD simulation yields $V_{eff} \sim 2.5 \times 10^{-3}\lambda^3$. This mode volume is reduced by a factor of ~10 compared to the air-slot cavity ($2.5 \times 10^{-2}\lambda^3$) in Fig. 1(b). This factor is only slightly smaller than the analytically predicted value of $\epsilon_h/\epsilon_l = 12.1$. If b is increased to 10 nm (40 nm), as shown in Fig. 1(d) [Fig. 1(e)], the mode volume expands to ~$4.3(7.7) \times 10^{-3}\lambda^3$. For all of these bridge widths, V_{eff} remains below that of the original slot cavity. As the bridge width is increased, V_{eff} also increases because of a weaker effect from type-2 BC [16]. We note that the fields outside the cavity region are nearly unchanged for these different near-field dielectric structures; i.e., they are nearly identical to Fig. 1(a) [16].

The small bridge dimensions require extremely memory-intensive and slow three-dimensional FDTD simulations because of the requirement for nanometer-scale meshing. However, provided that the cavity modes are nearly identical in the unperturbed region in Fig. 1(a), and the EM problem is quasistatic in the deeply subwavelength scale of the cavity center, is it even necessary to perform three-dimensional FDTD simulations to estimate the mode volume and fields? The bottom panels in Figs. 1(b)–1(e) plot the electric fields obtained by two-dimensional electrostatic simulations when an (arbitrary) potential difference ΔV is applied between the upper and lower boundaries [16]. These two-dimensional electrostatic simulations based on finite element methods (FEM) are several orders of magnitude faster than three-dimensional FDTD simulations. Remarkably, the $|E|$ distributions are very similar for the simple two-dimensional FEM and the laborious three-dimensional FDTD simulations, allowing a rapid exploration of the design space of the subwavelength dielectric structuring [16].

Combinations of type-1 and type-2 BCs open a wide design space. Introducing a low-index slot (i.e., exploiting the type-1 BC) changes the cavity from a dielectric-mode cavity into an air-mode cavity. Conversely, introducing a bridge (i.e., using the type-2 BC) changes the cavity from an air-mode cavity into a dielectric-mode cavity. As a result, alternate applications of slots (type-1 BC) and bridges

(type-2 BC) can continue reducing the mode volume. As a demonstration, Fig. 2(a) shows the cavity mode of a SBS cavity after the addition of an $s = 1$ nm slot (S) to the SB cavity design of Fig. 1(d), which reduces V_{eff} by ~7 times to $6.1 \times 10^{-4}\lambda^3$ (simulated with three-dimensional FDTD). The reduction is less than $\varepsilon_h/\varepsilon_l$ possible by the type-1 BC because of the finite slot width, but, in principle, an infinitesimal slot can achieve ~$\varepsilon_h/\varepsilon_l$ reduction.

Repeated concatenations with a fixed b_i/s_i, s_{i+1}/b_i ratio, where subscript i denotes the ith step of concatenation, produce a self-similar dielectric pattern in the cavity center. Arbitrary reduction of V_{eff} is possible in this limit (neglecting for the moment other practical issues discussed below). In the quasistatic limit (deep subwavelength), the electric field (energy density) is only determined by the boundary conditions and (relative) permittivity distribution $\epsilon(\vec{r})$, which both have scale invariance. Thus, the expanding symmetry of the self-similar permittivity distribution implies field distribution with an expanding symmetry. This means that the electric energy density increases exponentially with the number of concatenations, resulting in vanishing V_{eff}.

Practically, fabrication places limits on the minimum size of structures in a design, and concatenation is impossible at some point. Figure 2(b) shows the field concentration in a disconnected tip with a 45° taper angle, corresponding to a self-similar design with $b_i/s_i = 1$, $s_{i+1}/b_i = 1 - \delta$ ($i = 1$, $2...N$), $\delta \to +0$, $N \to \infty$ [16]. Assuming a radius of curvature of the tip of $r = 1$ nm and a tip gap of 1 nm, we estimate a mode volume of $V_{eff} = 7.0 \times 10^{-5}\lambda^3$. The panels on the right of Fig. 2 show the extreme field concentration in the horizontal (red) and vertical (blue) traces. Here we described an air-mode cavity with a disconnected tip, but the dielectric-mode cavity can also be implemented with connected tips. These designs with tip features have the advantages in fabrication because they are easier to be fabricated than small size, 90° bridges and slots.

Electron beam lithography followed by reactive ion etching [17,18], or focused ion beam milling [19], allows the patterning of dielectric tips with a gap below 10 nm. Alternatively, anisotropic etching of crystalline materials, such as wet etching of Si, can produce sharp tips with radius of curvature on the nanometer scale [20]. This method also has successfully demonstrated in-plane tip fabrication [21]. After, oxidation sharpening can be used, further reducing the radius of curvature to subnanometer [22]. Lastly, the fabrication requirements are more relaxed at longer wavelengths, such as in the midinfrared spectrum.

It is interesting to consider what happens if the tip radius r continues to be decreased. The field enhancement at a tip, with $r = 0$, is a well-studied problem in electrostatics, both for conductor [23] and dielectric [24] materials. The field at a dielectric tip, which can be expressed by a transcendental equation, diverges at the apex [24], which results in $V_{eff} = 0$, agreeing with our aforementioned proof. However, in this case, V_{eff} loses its physical meaning because the dipole approximation of the light-matter interaction no longer holds.

Do the sharp features of the field concentrator still permit a high Q factor in our cavity? Robinson *et al.* noted that introducing a slot significantly reduced the Q factor [12]. This reduction of Q can be interpreted from perturbation theory, as the radiation loss induced by the permittivity change $\Delta\epsilon(\vec{r})$ of the PhC structure. Fortunately, it is generally possible to cancel this radiation in the far field through additional perturbations elsewhere in the PhC structure [25]. In Fig. 3, we summarize our optimization of the Q factor of the fundamental cavity mode for successive introductions of slots and bridges (S, SB, and SBS), as well as for the tip design with 1 nm gap and $r = 1$ nm. We performed these radiation loss minimizations by three-dimensional FDTD, using particle swarm optimization for the length of the slot, the lattice constant, and the positions and radii of the holes symmetrically about the cavity center [16]. This process allowed us to maintain a high Q over 10^6 [Fig. 3(a)] across all mode concentration designs.

As shown in Fig. 3(b), the corresponding Q/V_{eff} values, in units of λ^{-3}, can exceed 10^{10}. It is useful to compare
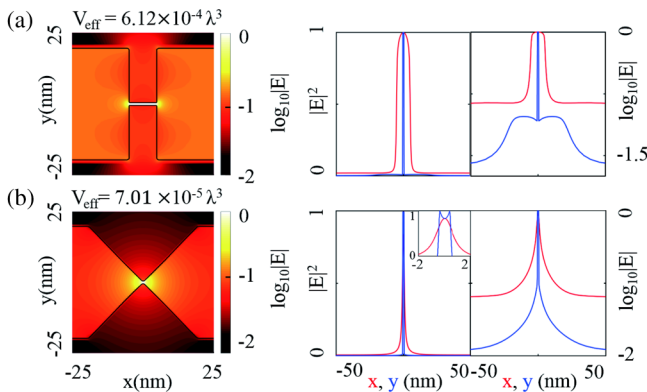
FIG. 2.   Electric field distribution. (a) Slot-bridge-slot (SBS) cavity. (b) Tip cavity as a limiting case of concatenation. Here, we show an air-mode cavity, and the tip is smoothed out. The two-dimensional field distribution in log scale (left). Field distribution along the line cut in linear scale (middle), and log scale (right). For the same reason as in Fig. 1, the field at the middle of the structure is used as a maximum for V_{eff} calculation. Note that the tip cavity has a higher field intensity at the tip than the middle in the inset.
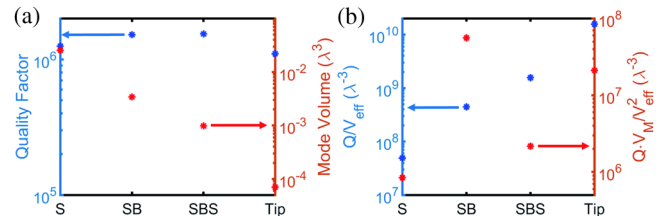
FIG. 3.   (a) Quality factors and mode volumes in each case after Q optimization: S cavity ($s_1 = 40$ nm); SB cavity ($b_1 = 10$ nm); SBS cavity ($s_2 = 3$ nm). Tip: Tip cavity (air-mode cavity, 1 nm gap, $r = 1$ nm) [16]. (b) Two figures of merit: Q/V_{eff} as a general criteria and QV_M/V_{eff}^2 for single-photon nonlinearities.

these Q/V_{eff} values with recently reported figures obtained by blind numerical optimizations, specifically, using an evolutionary algorithm (EA) [26], inverse design (ID) [27], and topology optimization (TO) [28]. These optimization approaches yielded Q/V_{eff} ratios of $\sim 1.0 \times 10^5$ (EA), $\sim 1.0 \times 10^6$ (ID), and $\sim 3.0 \times 10^7$ (TO). The corresponding mode volumes, in units of λ^3, were 0.01 (EA), 0.007 (ID), and 0.001 (TO). These results have practical limitations. The ID and TO approaches require a continuously varying refractive index (which is difficult for commonly used materials), and all approaches produced disconnected dielectric structures (difficult for fabrication).

Remarkably, in reviewing the optimized dielectric structures from these numerical approaches, one discovers a strikingly similar feature to our designs: two concentric tips centered at the cavity, which are disconnected for the EA approach and joined for the ID and TO approaches [16]. Our semianalytical analysis elucidates the origin of this feature. Optimizing this feature simplifies the design process to achieve higher Q and smaller V_{eff}, while ensuring a fully connected binary dielectric constant (that can be fabricated using standard lithography). Also, our design suggests that even smaller mode volume is possible with a (two-dimensional-tapered) conical tip.

Table I summarizes the figures of merit (FOM) that, in addition to Q/V_{eff}, are important for various applications, including spontaneous emission rate enhancement (Purcell effect) of quantum emitters, strong emitter-cavity coupling, optical bistability, and single-photon Kerr nonlinearities. All listed applications benefit from small V_{eff} and most benefit from high Q. Moreover, because Q factors are often practically limited (by material losses, scattering [29], or application-specific bandwidth constraints), reducing V_{eff} is particularly beneficial for many applications.

Specifically, we show here that the extreme field concentration can enable single-photon level Kerr nonlinearities at room temperature without an atomic medium or atomlike emitters, which are often difficult to fabricate and control. The Hamiltonian of a cavity with Kerr medium is expressed by [30]

TABLE I. Figures of merit for application areas of photonic nanocavities.

Application	Regime	FOM
Purcell effect	BC [a]	Q/V_{eff}
	BE [b]	$1/V_{\mathrm{eff}}$
Strong coupling	BC	$Q/\sqrt{V_{\mathrm{eff}}}$
with two level emitter	BE	$1/\sqrt{V_{\mathrm{eff}}}$
Optical bistability		Q^2/V_{Kerr} [c]
Single-photon Kerr nonlinearity		QV_M/V_{eff}^2 [d]

[a]Bad cavity.
[b]Bad emitter.
[c]$V_{\mathrm{Kerr}} = [(\int \epsilon |E|^2 dV)^2 \max(n_2/\epsilon)]/$
    $[\int (n_2 \epsilon/3)(|EE|^2 + 2|E|^4)dV]$ [25].
[d]$V_M = [\int_M |E(\vec{r})|^4 dV]/[\max(|E(\vec{r})|^4)]$.

$$H = [\hbar\omega - i\kappa/2 + \eta(\hat{n} - 1)]\hat{n}, \qquad (7)$$

where $\kappa = \omega/Q$ is the cavity linewidth, and η is the one-photon resonance frequency shift. η can be derived from perturbation theory [16],

$$\frac{\eta}{\omega} = -\frac{3\chi^{(3)}\hbar\omega}{4\epsilon_0\epsilon^2}\frac{V_M}{V_{\mathrm{eff}}^2}, \qquad (8)$$

where $V_M = \int_M |E(\vec{r})|^4 dV / \max(|E(\vec{r})|^4)$, and the integration is over the region of nonlinear medium (M). The term $|E(\vec{r})|^4$ is due to the mode overlap ($\propto |E(\vec{r})|^2$) and the Kerr index shift ($\propto |E(\vec{r})|^2$). In our simulations, V_M approximates the volume of the region of highest field concentration feature (the slot, bridge, or gap between the tip).

The condition for a single photon to shift the cavity by one resonance linewidth is [16]

$$\frac{QV_M}{V_{\mathrm{eff}}^2} > \frac{4\epsilon_0}{3\hbar\omega}\frac{\epsilon^2}{|\chi^{(3)}|}, \qquad (9)$$

assuming that the cavity radiation loss dominates over material losses (see Supplemental Material for a discussion on material loss [16]). Under this condition, photons in the cavity can be considered as strongly interacting particles [31]. The required $|\chi^{(3)}|/\epsilon^2$ is $\sim 1.60 \times 10^{-17}$ m^2/V^2 for the tip cavity design in Fig. 3. This type of Kerr nonlinearity is possible with organic materials that could be conveniently introduced into the air slot of the cavity. The J aggregate (PIC) has $|\chi^{(3)}|/\epsilon^2 = 1.1 \times 10^{-15}$ m^2/V^2 at $\lambda = 575$ nm [32]; PTS-polydiacetylene has $|\chi^{(3)}|/\epsilon^2 = -0.931 \times 10^{-17}$ m^2/V^2 at $\lambda = 1060$ nm [33]. Inorganic materials that can be deposited by atomic layer deposition are also promising for direct introduction into the slot area; indium tin oxide, for example, has been reported to have $|\chi^{(3)}|/\epsilon^2 = 2.12 \times 10^{-17}$ m^2/V^2 at $\lambda = 1175$ nm [34].

The proposed bridge cavity requires $|\chi^{(3)}|/\epsilon^2 \sim 0.61 \times 10^{-17}$ m^2/V^2 to reach a single-photon nonlinearity. Conventional semiconductor materials such as Si (0.99×10^{-19} m^2/V^2) [35–37], GaAs (0.97×10^{-20} m^2/V^2, at $\lambda = 1.06$ um) [38], and Ge (0.86×10^{-20} m^2/V^2, at $\lambda = 3.17$ um) [39] do not meet this requirement, but could nevertheless produce a strong nonlinearity at extremely low powers (corresponding to a few hundreds of photons in the cavity). These parametric few-photon nonlinearities could have numerous applications in frequency conversion [40], all-optical memory, logic, and routing [41–43], neuromorphic optical computing [44,45], and entangled photon pair production by spontaneous four-wave mixing [46–48].

In conclusion, we have introduced a recipe for the ultrasmall mode volume dielectric cavity. We proposed a tip cavity structure and reviewed optimization results reported. Remarkably, the extreme field concentration enabled by these dielectric features greatly amplifies nonlinear optical interactions. For realistic dielectric materials, a full cavity linewidth shift appears to be possible even for a

single photon within the cavity. The ultrastrong light-matter interaction opens the door to new applications feasible even at room temperature: ultrastrong Purcell enhancement [49], single molecule sensing [7], cavity QED [50], optomechanics [51], and quantum nonlinear optics [52].

Note added.—Recently, we became aware of another similar design [53].

[*]choihr@mit.edu
[†]englund@mit.edu

[1] K. J. Vahala, Optical microcavities, Nature (London) **424**, 839 (2003).

[2] H. Altug, D. Englund, and J. Vučković, Ultrafast photonic crystal nanocavity laser, Nat. Phys. **2**, 484 (2006).

[3] S. Matsuo, A. Shinya, T. Kakitsuka, K. Nozaki, T. Segawa, T. Sato, Y. Kawaguchi, and M. Notomi, High-speed ultra-compact buried heterostructure photonic-crystal laser with 13 fj of energy consumed per bit transmitted, Nat. Photonics **4**, 648 (2010).

[4] M. Lončar, T. Yoshie, A. Scherer, P. Gogna, and Y. Qiu, Low-threshold photonic crystal laser, Appl. Phys. Lett. **81**, 2680 (2002).

[5] D. Englund, A. Faraon, I. Fushman, N. Stoltz, P. Petroff, and J. Vučković, Controlling cavity reflectivity with a single quantum dot, Nature (London) **450**, 857 (2007).

[6] T. G. Tiecke, J. D. Thompson, N. P. de Leon, L. R. Liu, V. Vuletić, and M. D. Lukin, Nanophotonic quantum phase switch with a single atom, Nature (London) **508**, 241 (2014).

[7] A. M. Armani, R. P. Kulkarni, S. C. Fraser, R. C. Flagan, and K. J. Vahala, Label-free, single-molecule detection with optical microcavities, Science **317**, 783 (2007).

[8] M. Soljačić and J. D. Joannopoulos, Enhancement of nonlinear effects using photonic crystals, Nat. Mater. **3**, 211 (2004).

[9] K. Nozaki, T. Tanabe, A. Shinya, S. Matsuo, T. Sato, H. Taniyama, and M. Notomi, Subfemtojoule all-optical switching using a photonic-crystal nanocavity, Nat. Photonics **4**, 477 (2010).

[10] R. Pant, E. Li, D.-Y. Choi, C. G. Poulton, S. J. Madden, B. Luther-Davies, and B. J. Eggleton, Cavity enhanced stimulated Brillouin scattering in an optical chip for multiorder stokes generation, Opt. Lett. **36**, 3687 (2011).

[11] Y. Takahashi, H. Hagino, Y. Tanaka, B. S. Song, T. Asano, and S. Noda, High-q nanocavity with a 2-ns photon lifetime, Opt. Express **15**, 17206 (2007).

[12] J. T. Robinson, C. Manolatou, L. Chen, and M. Lipson, Ultrasmall Mode Volumes in Dielectric Optical Microcavities, Phys. Rev. Lett. **95**, 143901 (2005).

[13] P. T. Kristensen, C. Van Vlack, and S. Hughes, Generalized effective mode volume for leaky optical cavities, Opt. Lett. **37**, 1649 (2012).

[14] R. Coccioli, M. Boroditsky, K. W. Kim, Y. Rahmat-Samii, and E. Yablonovitch, Smallest possible electromagnetic mode volume in a dielectric cavity, IEEE Proc. **145**, 391 (1998).

[15] P. Seidler, K. Lister, U. Drechsler, J. Hofrichter, and T. Stöferle, Slotted photonic crystal nanobeam cavity with an ultrahigh quality factor-to-mode volume ratio, Opt. Express **21**, 32468 (2013).

[16] See Supplemental Material at http://link.aps.org/supplemental/10.1103/PhysRevLett.118.223605, which includes Refs. [54–59], for bridge width dependence of mode volume, field profiles, two-dimensional electrostatic simulation, stair-case approximation of tips, quality factor optimization, previous numerical optimization results, derivation of line shift induced by Kerr effect, and material losses.

[17] C. M. Hsu, S. T. Connor, M. X. Tang, and Y. Cui, Wafer-scale silicon nanopillars and nanocones by Langmuir-Blodgett assembly and etching, Appl. Phys. Lett. **93**, 133109 (2008).

[18] G. Villanueva, J. A. Plaza, A. Sánchez-Amores, J. Bausells, E. Martínez, J. Samitier, and A. Errachid, Deep reactive ion etching and focused ion beam combination for nanotip fabrication, Mater. Sci. Eng. C **26**, 164 (2006).

[19] L. Novotny and N. Van Hulst, Antennas for light, Nat. Photonics **5**, 83 (2011).

[20] B. Tang and K. Sato, Formation of silicon nanotips in surfactant-modified wet anisotropic etching, Appl. Phys. Express **4**, 056501 (2011).

[21] D. Saya, T. Leïchlé, J. B. Pourciel, C. Bergaud, and L. Nicu, Collective fabrication of an in-plane silicon nanotip for parallel femtoliter droplet deposition, J. Micromech. Microeng. **17**, N1 (2007).

[22] R. B. Marcus, T. S. Ravi, T. Gmitter, K. Chin, D. Liu, W. J. Orvis, D. R. Ciarlo, C. E. Hunt, and J. Trujillo, Formation of silicon tips with < 1 nm radius, Appl. Phys. Lett. **56**, 236 (1990).

[23] J. D. Jackson, *Classical Electrodynamics* (Wiley, New York, 1999).

[24] J. Andersen and V. Solodukhov, Field behavior near a dielectric wedge, IEEE Trans. Antennas Propag. **26**, 598 (1978).

[25] J. D. Joannopoulos, S. G. Johnson, J. N. Winn, and R. D. Meade, *Photonic Crystals: Molding the Flow of Light* (Princeton University Press, Princeton, NJ, 2011).

[26] A. Gondarenko and M. Lipson, Low modal volume dipole-like dielectric slab resonator, Opt. Express **16**, 17689 (2008).

[27] J. Lu, S. Boyd, and J. Vučković, Inverse design of a three-dimensional nanophotonic resonator, Opt. Express **19**, 10563 (2011).

[28] X. Liang and S. G. Johnson, Formulation for scalable optimization of microcavities via the frequency-averaged local density of states, Opt. Express **21**, 30812 (2013).

[29] X. Ji, F. A. S. Barbosa, S. P. Roberts, A. Dutt, J. Cardenas, Y. Okawachi, A. Bryant, A. L. Gaeta, and M. Lipson, Breaking the loss limitation of on-chip high-confinement resonators, arXiv:1609.08699.

[30] M. Gullans, D. E. Chang, F. H. L. Koppens, F. J. G. de Abajo, and M. D. Lukin, Single-Photon Nonlinear Optics with Graphene Plasmons, Phys. Rev. Lett. **111**, 247401 (2013).

[31] A. Imamoglu, H. Schmidt, G. Woods, and M. Deutsch, Strongly Interacting Photons in a Nonlinear Cavity, Phys. Rev. Lett. **79**, 1467 (1997).

[32] F. A. Zhuravlev, N. A. Orlova, V. V. Shelkovnikov, A. I. Plekhanov, S. G. Rautian, and V. P. Safonov, Giant nonlinear susceptibility of thin films with (molecular j-aggregate)-(metal cluster) complexes, Sov. J. Exp. Theor. Phys. Lett. **56**, 260 (1992).

[33] D. M. Krol and M. Thakur, Measurement of the nonlinear refractive index of single-crystal polydiacetylene channel waveguides, Appl. Phys. Lett. **56**, 1406 (1990).

[34] M. Z. Alam, I. De Leon, and R. W. Boyd, Large optical nonlinearity of indium tin oxide in its epsilon-near-zero region, Science **352**, 795 (2016).

[35] H. Yamada, M. Shirane, T. Chu, H. Yokoyama, S. Ishida, and Y. Arakawa, Nonlinear-optic silicon-nanowire waveguides, Jpn. J. Appl. Phys. **44**, 6541 (2005).

[36] H. K. Tsang and Y. Liu, Nonlinear optical properties of silicon waveguides, Semicond. Sci. Technol. **23**, 064007 (2008).

[37] J. Leuthold, C. Koos, and W. Freude, Nonlinear silicon photonics, Nat. Photonics **4**, 535 (2010).

[38] L. L. Chase, E. W. Van Stryland, and M. J. Weber, *Handbook of Laser Science and Technology Supplement* (CRC Press, Boca Raton, FL, 1995).

[39] N. K. Hon, R. Soref, and B. Jalali, The third-order nonlinear optical coefficients of SI, GE, and SIGE in the midwave and longwave infrared, J. Appl. Phys. **110**, 011301 (2011).

[40] B. Corcoran, C. Monat, C. Grillet, D. J. Moss, B. J. Eggleton, T. P. White, L. O'Faolain, and T. F. Krauss, Green light emission in silicon through slow-light enhanced third-harmonic generation in photonic-crystal waveguides, Nat. Photonics **3**, 206 (2009).

[41] K. Nozaki, A. Shinya, S. Matsuo, Y. Suzaki, T. Segawa, T. Sato, Y. Kawaguchi, R. Takahashi, and M. Notomi, Ultra-low-power all-optical ram based on nanocavities, Nat. Photonics **6**, 248 (2012).

[42] K. Nozaki, T. Tanabe, A. Shinya, S. Matsuo, T. Sato, H. Taniyama, and M. Notomi, Subfemtojoule all-optical switching using a photonic-crystal nanocavity, Nat. Photonics **4**, 477 (2010).

[43] M. P. Fok and P. R. Prucnal, All-optical encryption based on interleaved waveband switching modulation for optical network security, Opt. Lett. **34**, 1315 (2009).

[44] Y. Shen, N. C. Harris, S. Skirlo, M. Prabhu, T. Baehr-Jones, M. Hochberg, X. Sun, S. Zhao, H. Larochelle, D. Englund, and M. Soljacic, Deep learning with coherent nanophotonic circuits, arXiv:1610.02365.

[45] A. N. Tait, E. Zhou, T. F. de Lima, A. X. Wu, M. A. Nahmias, B. J. Shastri, and P. R. Prucnal, Neuromorphic silicon photonics, arXiv:1611.02272.

[46] H. Takesue and K. Inoue, Generation of polarization-entangled photon pairs and violation of bells inequality using spontaneous four-wave mixing in a fiber loop, Phys. Rev. A **70**, 031802 (2004).

[47] R. M. Camacho, Entangled photon generation using four-wave mixing in azimuthally symmetric microresonators, Opt. Express **20**, 21977 (2012).

[48] S. F. Preble, M. L. Fanto, J. A. Steidle, C. C. Tison, G. A. Howland, Z. Wang, and P. M. Alsing, On-chip quantum interference from a single silicon ring-resonator source, Phys. Rev. Applied **4**, 021001 (2015).

[49] M. Boroditsky, R. Vrijen, T. F. Krauss, R. Coccioli, R. Bhat, and E. Yablonovitch, Spontaneous emission extraction and purcell enhancement from thin-film two-dimensional photonic crystals, J. Lightwave Technol. **17**, 2096 (1999).

[50] T. Yoshie, A. Scherer, J. Hendrickson, G. Khitrova, H. M. Gibbs, G. Rupper, C. Ell, O. B. Shchekin, and D. G. Deppe, Vacuum rabi splitting with a single quantum dot in a photonic crystal nanocavity, Nature (London) **432**, 200 (2004).

[51] M. Eichenfield, J. Chan, R. M. Camacho, K. J. Vahala, and O. Painter, Optomechanical crystals, Nature (London) **462**, 78 (2009).

[52] D. E. Chang, V. Vuletić, and M. D. Lukin, Quantum nonlinear optics photon by photon, Nat. Photonics **8**, 685 (2014).

[53] S. Hu and S. M. Weiss, Design of photonic crystal cavities for extreme light concentration, ACS Photonics **3**, 1647 (2016).

[54] J. Larsson, Electromagnetics from a quasistatic perspective, Am. J. Phys. **75**, 230 (2007).

[55] A. Taflove and S. C. Hagness, *Computational Electrodynamics* (Artech House Publishers, Melville, NY, 2000).

[56] G. V. Naik, J. Kim, and A. Boltasseva, Oxides and nitrides as alternative plasmonic materials in the optical range, Opt. Mater. Express **1**, 1090 (2011).

[57] S. Valleau, S. K. Saikin, M. Yung, and A. A. Guzik, Exciton transport in thin-film cyanine dye *j* aggregates, J. Chem. Phys. **137**, 034109 (2012).

[58] A. K. Bhowmik and M. Thakur, Self-phase modulation in polydiacetylene single crystal measured at 720–1064 nm, Opt. Lett. **26**, 902 (2001).

[59] M. Thakur, R. C. Frye, and B. I. Greene, Nonresonant absorption coefficient of single-crystal films of polydiacetylene measured by photothermal deflection spectroscopy, Appl. Phys. Lett. **56**, 1187 (1990).